Decameter structure in heater-induced airglow at the High frequency Active Auroral Research Program facility

Elizabeth Kendall,[1] Robert Marshall,[2] Richard Todd Parris,[3] Asti Bhatt,[4] Anthea Coster,[4] Todd Pedersen,[5] Paul Bernhardt,[6] and Craig Selcher[6]

Received 30 October 2009; revised 19 February 2010; accepted 25 March 2010; published 10 August 2010.

[1] On 28 October 2008, small-scale rayed artificial airglow was observed at the High frequency Active Auroral Research Program (HAARP) heating facility by the HAARP telescopic imager. This airglow occurred during an experiment at twilight from 0255–1600 UT (1855–2000 LT) and with estimated scale sizes of 100 m (at assumed 225 km altitude) constitutes the smallest structure observed in artificial airglow to date. The rays appeared to be oriented along the geomagnetic field lines. During this period, other instruments, SuperDARN, GPS receivers, stimulated electromagnetic emissions receivers, also recorded unusual data sets with the general characteristic of time scales longer than anticipated for features to form. The experiment took place at the commencement of a small geomagnetic disturbance (*Kp* of 4.3). This unique observation is as yet unexplained. The airglow features start as large scale structures and then become smaller as heating continues in apparent contradiction to current theories on irregularity development. A thermal gradient instability at boundary of the ionospheric footprint of the plasmapause may be responsible for causing the small-scale structuring. Observations of 427.8 nm N_2^+ (first negative group) emissions indicate the presence of ionization.

Citation: Kendall, E., R. Marshall, R. T. Parris, A. Bhatt, A. Coster, T. Pedersen, P. Bernhardt, and C. Selcher (2010), Decameter structure in heater-induced airglow at the High frequency Active Auroral Research Program facility, *J. Geophys. Res.*, *115*, A08306, doi:10.1029/2009JA015043.

1. Background

[2] Ionospheric optical emissions generated by high-power HF transmitters, or "heaters," have been studied by the ionospheric physics community for several decades. Labeled "artificial airglow" or "artificial aurora," these emissions are at a basic level caused by radio waves accelerating electrons into collisions with neutral species, which then either emit a photon through an excitation process or possibly become ionized. This interaction generally occurs at or near a resonance in the ionosphere where the radio wave interacts strongly with the plasma. Optical emissions have been recorded between ~110 and 300 km altitude and span both the E and F regions of the ionosphere, although *F* region emissions by far comprise the bulk of observations. The most commonly observed emissions are characteristic of atomic oxygen and molecular nitrogen since these are the primary constituents of the upper atmosphere at these altitudes.

[3] Early artificial airglow studies were conducted at heating facilities in Platteville, Colo [*Biondi et al.*, 1970; *Sipler and Biondi*, 1972]; in Moscow, Russia [*Adeishvili et al.*, 1979]; and in Arecibo, Puerto Rico [*Sipler et al.*, 1974]. Later studies were conducted in Tromsø, Norway (European Incoherent Scatter (EISCAT)) [*Stubbe et al.*, 1982; *Brändström et al.*, 1999]; in Vasilsursk, Russia (Sura) [*Bernhardt et al.*, 1991]; and in Gakona, Alaska (High frequency Active Auroral Research Program (HAARP)) [*Pedersen and Carlson*, 2001]. The data presented in this paper were all collected at the HAARP facility. HAARP is a high-frequency (HF) phased antenna array located in Alaska (62.4°N, 145.1°W) and is jointly managed by the Air Force Research Laboratory and the Office of Naval Research. The original prototype was built in 1994 with the full 180 crossed dipole array completed in 2006. The antenna operates from 2.8 to 10 MHz with 3.6 MW transmitted power. At 2.8 MHz, the beam width is 15.9° East-West and 20.2° North-South with an effective power at the beam center of 84.1 dBW.

[4] Enhanced O(^1D) 630.0 nm and, to a lesser degree, O(^1S) 557.7 nm airglow emissions have been most commonly observed at these facilities in response to heating. At high latitudes the airglow region is frequently displaced toward magnetic zenith (along the geomagnetic field lines), even when the heating beam is aimed in the true zenith direction. This displacement toward magnetic zenith was first observed at Tromsø [*Kosch et al.*, 2000] and then at HAARP [*Pedersen and Carlson*, 2001]. An artificial airglow cam-

[1]SRI International, Menlo Park, California, USA.
[2] Stanford University, Stanford, California, USA.
[3] University of Alaska, Fairbanks, Alaska, USA.
[4]Massachusetts Institute of Technology Haystack Observatory, Westford, Massachusetts, USA.
[5] Air Force Research Laboratory, Hanscom AFB, Massachusetts, USA.
[6]Naval Research Laboratory, Washington, DC, USA.

0148-0227/10/2009JA015043

paign was conducted at HAARP from 31 January to 19 February 2002 during which the heater beam was aimed along the geomagnetic field lines and a dramatic enhancement in airglow brightness was observed [*Pedersen et al.*, 2003]. Bright 630 nm (several hundred Rayleighs) and 557.7 nm (over 50 R) airglow were recorded simultaneously during *F* layer heating. Several other wavelengths have also been observed on occasion in airglow emissions, e.g., O I 777.4 nm, O I 844.6 nm, N_2^+(1 NG) 427.8 nm, and, very rarely, the N_2(first positive (1 P)) 710–760 nm band [*Sentman et al.*, 2002; *Holma et al.*, 2006; *Gustavsson et al.*, 2006; *Djuth et al.*, 1999].

[5] HF heater-induced artificial airglow observations can be used to diagnose electron energies and distributions in the heated region, determine E × B plasma drifts [*Bernhardt et al.*, 1989], and measure quenching rates by neutral species. Airglow imaging allows measurements of spatial features in the optical emissions, which are presumably related to heater-illuminated natural and/or artificially induced ionospheric irregularities. Unlike the typically smooth electron density variations at equatorial and middle latitudes, the lower ionosphere at high latitudes is in general turbulent, with many natural electron density perturbations, or irregularities, present [e.g., *Kelley*, 1989, p. 345]. These irregularities, typically regions of electron depletion, lead to a rich environment of wave-wave and wave-particle plasma interactions, many of which are not yet fully understood. Irregularities can lead to practical issues, such as the scintillation of satellite signals, and are of great interest to those attempting to develop better space-Earth communications. Rocket data show that heater-induced irregularities consist of bundles of ~10 m wide magnetic field-aligned filaments with a mean depletion depth of 6% [*Kelley et al.*, 1995]. These bundles themselves constitute small-scale structures with widths of 1.5 to 6 km. A separate rocket experiment released CF_3Br in the ionosphere, and waves trapped in decameter-scale density depletions during heating were similarly observed [*Rodriguez et al.*, 1995].

[6] With the advent of modern CCD detectors, structure in artificial airglow has been observed at multiple heating facilities. *Gustavsson et al.* [2001] report patchy 5 to 15 km, 630.0 nm airglow structures in the first ~20 s after the HF pump at the EISCAT heating facility is turned on. Large-scale (~20 km) moving features were observed in SURA 630.0 nm airglow data [*Bernhardt et al.*, 2000], and 10 km structures were observed in the 557.7 nm oxygen line at Arecibo in connection with *E* layer experiments [*Kagan et al.*, 2000]. Novel annular rings of order 60 km were observed to collapse and descend at the EISCAT high-gain HF facility [*Kosch et al.*, 2004]. The HAARP telescopic imager has the unique ability to detect structure on the order of tens of meters and has recorded the smallest-scale features to date as described in the following section.

2. Airglow Observations

[7] Telescopic observations of heater-induced airglow have been conducted at the HAARP heating facility since the spring of 2000. Originally carried out by Stanford University using a simple Dobsonian telescope and a trapdoor in the ceiling, the HAARP telescope is now housed in a ~4.3 meters dome and uses a robotic mount (Paramount ME from Software Bisque) for steering. The system consists of two imagers and a set of optics for each. The cameras and optics are identical except that one has a wide-angle lens (~19° field of view) and the other has a telescopic lens (~3° field of view). This allows a fine-scale resolution of ~20 m in the *F* layer and ~10 m in the *E* layer so that decameter and kilometer scale structures are readily observed. Both imagers use Princeton VersArray 512B CCD cameras, which are thermoelectrically cooled to −40°C with telecentric optics and temperature-controlled filter wheels. These cameras have a resolution of 512 × 512 pixels with 16-bit depth. In 2008, this system was upgraded to be remotely controllable. Although structured airglow was recorded by the telescope on a few occasions before HAARP's completion, fine structure in airglow is now observed on a regular basis. We here present the smallest-scale structure we have observed to date.

[8] A fall campaign was held at HAARP 25 October to 3 November 2008 focusing on ionospheric irregularities and optical emissions. On multiple nights, the HAARP telescope recorded fine structure at the 557.7 and 427.8 nm wavelengths. The night of 28 October proved to have especially small artificial airglow structure, on the scale of 100 m width, during an experiment running from 0255–0400 UT (1855–2000 LT). For this experiment, HAARP was operated at full CW power in *O* mode, aimed along the geomagnetic field lines at "magnetic zenith" (202° azimuth, 76° elevation). Operation in *O* mode (left-hand circular polarization) allows the wave to reach the reflection altitude and interact where the HF is equal to the local plasma frequency. The heater transmitted at 2.85 MHz with a repeating power cycle of 2 min on, 2 min off. 2.85 MHz is the second gyroharmonic frequency at ~225 km altitude. The fields of view of the HAARP telescope cameras, as well as other instruments in operation on 28 October at 250 km altitude, are shown in Figure 1.

[9] Figure 2 shows the estimated altitudes of resonant frequencies during the heating experiment, based on ionosonde data. The circles indicate altitudes where the local plasma frequency equals the heating frequency of 2.85 MHz. The plus signs show the altitudes where the calculated upper hybrid frequency equals 2.85 MHz. The solid horizontal line indicates the altitude above HAARP where the second electron gyroharmonic frequency is 2.85 MHz. The vertical gray bars mark the intervals where the heater was turned on. Several of the ionograms collected during this experiment could be interpreted as having multiple layers when the heater was on. The concept of "artificial ionization layers" is described in the study of *Pedersen et al* [2010]. In addition to the nighttime *F* layer, there were indications of two layers at lower altitudes, the lowest of which was ~150 km. Because the ionosonde readings were not lined up with the on and off cycles of the experiment, these additional patches of ionization do not show up in the majority of the ionograms.

[10] While kilometer-scale structure has been observed by the HAARP telescope on multiple nights, this night was unique in the presence of rayed structures with decameter widths. An example of typical airglow structure and morphology from previous campaign is given in the study of *Djuth et al.* [2005]. Because there was no side-viewing imagery at the time of this experiment, it is difficult to put a precise width on the rays. The ionograms recorded during

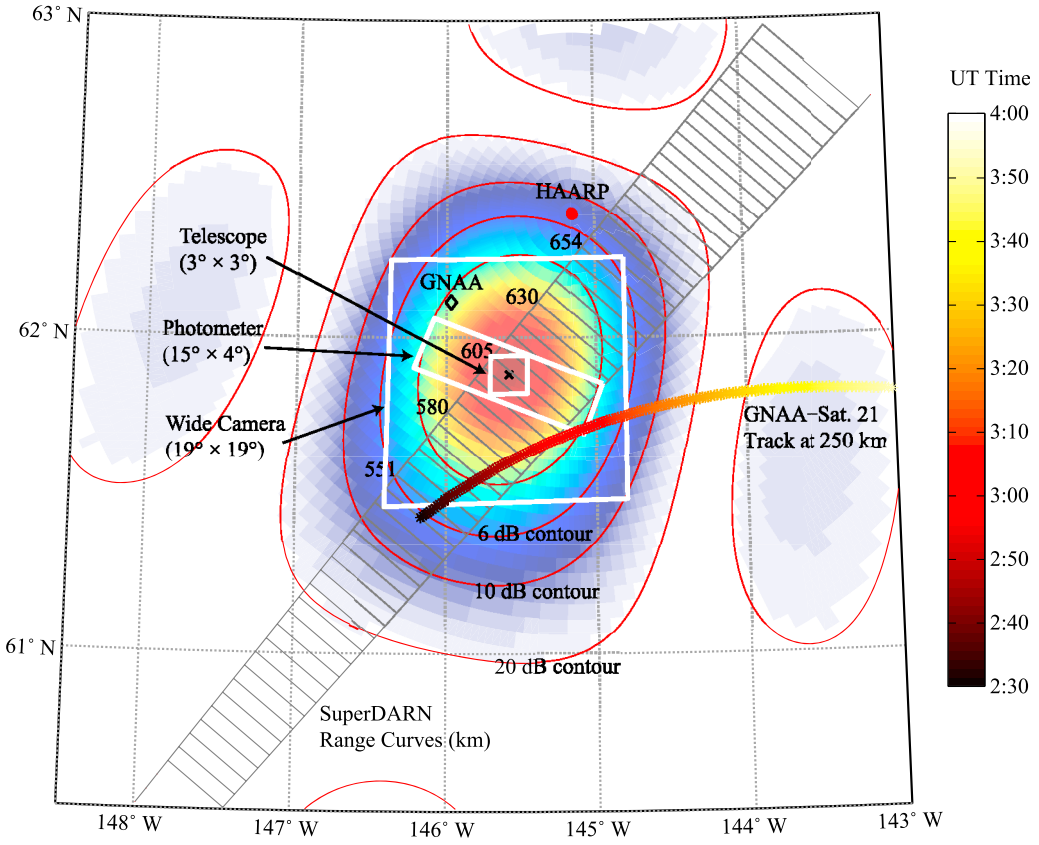

Figure 1. The relative positions of the fields of view for various instruments mapped to 250 km altitude. The telescope overlaps the wide field camera, the photometer, and beam 9 of the SuperDARN radar. The GNAA station receiver recorded GPS satellite 21 during the heating experiment. The color bar on the side shows the satellite track as a function of time. The HAARP beam contours are plotted in red.

the experiment indicate the presence of three layers. On the basis of the ionosonde-derived profiles, it is likely that the structures occurred at ~225, ~200, or ~160 km (the resonance altitudes of the three layers present). This gives minimum widths of ~70 m if 225 km altitude is assumed down to ~50 m if 160 km altitude is assumed. The rays appear to emanate from magnetic zenith and be oriented along the geomagnetic field lines as shown in Figure 3. The images were taken with the 557.7 nm filter and 1 s exposure.

[11] The rayed structures displayed in Figure 3 were frequently preceded by fainter, more diffuse patches with scale sizes on the order of a few kilometers or more. While these large, faint patches are clearly seen in movies of the airglow data, they are not as obvious as in still frames and hence not included in this paper. The two types of airglow are also observed in the photometer data and are presented in the discussion of Figure 4. The rays typically developed about 20–40 s into the heating cycle, whereas the more diffuse structures occurred immediately (within seconds of turn-on). In the wide field of view camera (~19°), the spatial extent of the diffuse region is more apparent. During each heating pulse, the diffuse region typically begins as a circular structure with a relatively sharp boundary approximately 70 km across and then shrinks toward the magnetic zenith as the rays begin to develop. This collapse could either indicate an actual change in spatial extent across the sky or a lifting of the airglow to higher altitudes, although it is not possible to determine the altitude variation definitively because of lack of additional data. Previous observations of rings collapsing into "blobs" at the EISCAT heating facility indicate that in fact the airglow was descending in altitude while collapsing as the heating caused an increase in electron temperature and lowered the reflection altitude [*Ashrafi et al.*, 2007]. Recent observations at HAARP have also shown large bright patches forming within rings which then collapse and descend to altitudes of ~150 km [*Pedersen et al.*, 2010]. It is possible that the 28 October images are similarly showing a descending collapse since an increase in plasma density at an apparent altitude of 225 km was observed (as evidenced by GPS total electron content (TEC) data in Figure 8) [*Ashrafi et al.*, 2006] as well as the formation of artificial layers on the bottomside *F* layer on the ionograms. The end of the experiment (~0345 UT) marks a shift in the airglow region from being centered around the magnetic zenith to a lower elevation and azimuth, roughly 185° azimuth and 74.5° elevation.

[12] The presence of the more diffuse, faint structure followed by brighter rays indicates that two airglow processes are in place. Figure 4 shows data from the HAARP photometer, operated by Stanford University. This photometer has a six-position filter wheel to routinely monitor airglow at multiple wavelengths with a cadence higher than

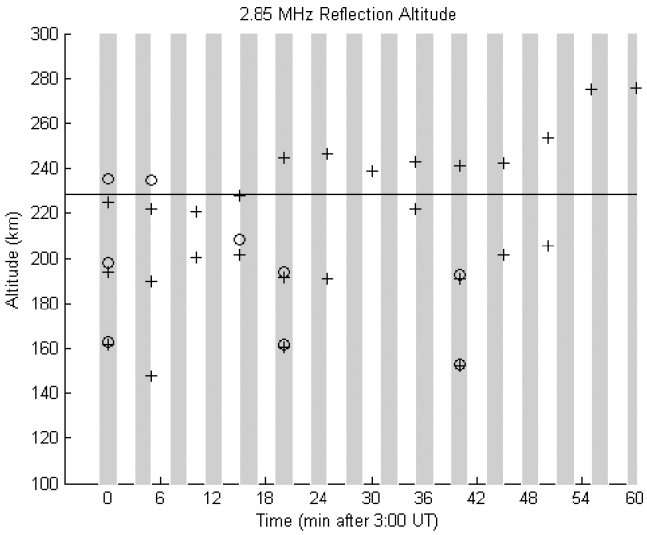

Figure 2. Altitudes of critical resonant frequencies based on ionosonde data. The circles represent the modeled altitude of reflection for 2.85 MHz, the heating frequency during this experiment. The plus signs show the altitude where the upper hybrid frequency equals 2.85 MHz. The solid horizontal line is located at the altitude where the second electron gyroharmonic frequency is equal to 2.85 MHz. The vertical gray bars represent the HAARP on periods. The ionograms were modeled with three layers and so there are frequently multiple altitudes of resonance at any one point in time.

most imaging data. The photometer is outfitted with a 50 mm camera lens, yielding a 14.8° × 4.2° field of view and 10 nm bandwidth optical filters. Data are sampled at 2500 samples per second, but the filter wheel hovers on each of six positions for 1 s at a time, yielding 6 s resolution in each wavelength. Of particular interest is the 557.7 nm filter data set since this matches the airglow observations. There appear to be two rise time constants present, one at the initial turn-on and then a second peak midway through the on cycle. These two time constants are consistent with the appearance of faint diffuse structures and then the brighter rayed structures in the telescope airglow images. This pattern also shows up in the 777.4 and 844.6 nm data. The 427.8 data, however, initially shows a sharp initial peak that slowly falls until a sharp drop-off at the end of the pulse. After 0335 UT, the pattern reverses to a rising pulse. Varying time scales were also observed in other data sets as discussed in the following section.

[13] In addition to varying over the period of a heater-on cycle, the airglow also changes throughout the hour of the experiment. Initially, the diffuse patches are not evident and only the bright rays are visible. The first hints of patches occur at 0308 UT, but this is most likely due to the twilight when the background light level is still very high, so only the brightest features are observable. From 0308 UT until 0347 UT, the overall pattern of faint patches and bright rays remains the same. At 0347 UT, the airglow occupies a smaller region of the sky and moves to the southeast, as evidenced in the wide field of view camera. The patches are also less apparent. After 0354 UT, there is no obvious airglow in the imagers and the experiment ends at 0400 UT. These transitions can be easily seen in the photometer data.

[14] While for the most part, the airglow observed by the telescope can be lumped into either a bright ray or a diffuse patch category, some additional morphological categories can be discerned in the images. One such category is clumps of rays that were sometimes observed to move in arcs across the images as shown in the series in Figure 5.

[15] While the limitations imposed by the observation frame rate make detailed analysis of the metamorphosis of individual airglow structures difficult, in some cases, the features did persist for multiple frames. In these cases the direction and velocity of the features can be estimated. In one case a "bead" feature, most likely a ray extending along the magnetic field lines viewed from directly below, appeared to break into two beads. One of these beads then traveled to the magnetic north at ~50 m/s if all motion is assumed to occur in a plane parallel to the image plane at an altitude of 160 km (or ~70 m/s at 225 km altitude).

3. Data Comparison

[16] The bright rayed structure observed on 28 October 2008 was the smallest-scale heater-induced structure

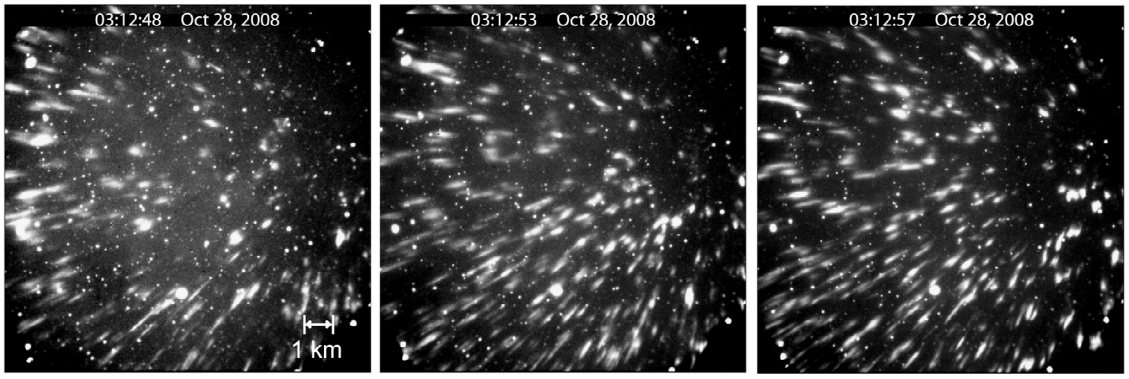

Figure 3. Three images from the HAARP telescope, showing bright rayed structure on the 100 meter scale. A 1 km scale is shown in the lower right of the first image. The rays appear to be field aligned. The images were exposed for 1 s at 557.7 nm.

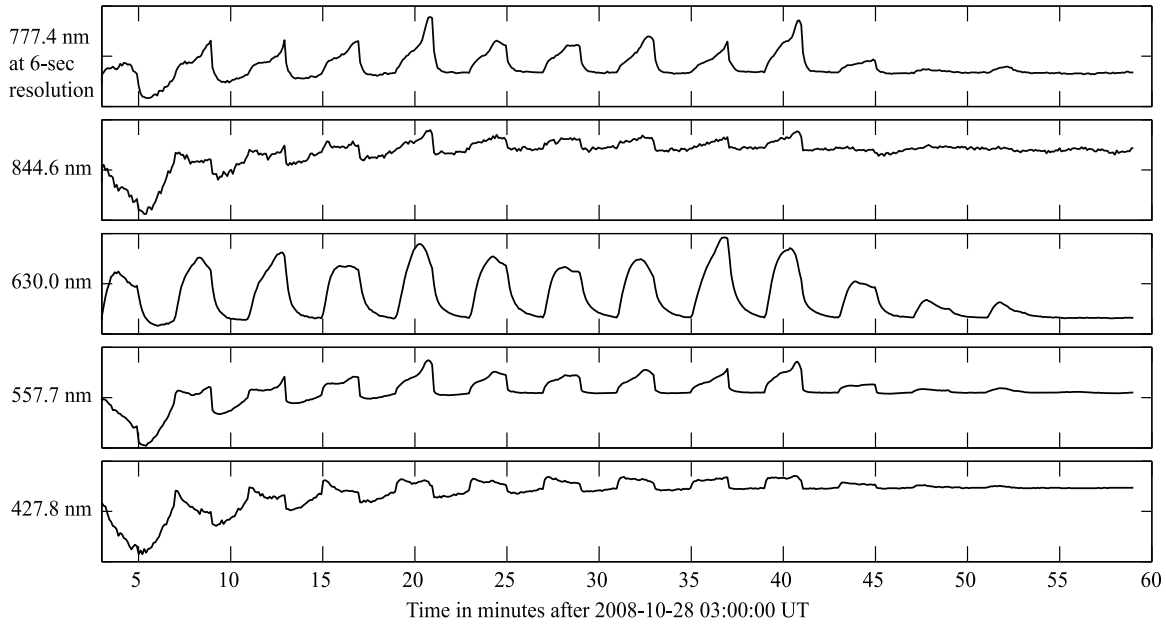

Figure 4. Data from the Stanford/HAARP photometer showing airglow intensities during the 28 October event. The data have been background-subtracted which accounts for the large dip at the beginning of the data set (during bright twilight). The heating cycles appear in the 777.4, 844.6, 630.0, 557.7, and 427.8 nm wavelength filters. The 557.7 nm data show multiple time constants, which appear to be related to the varying airglow morphology seen by the imagers.

observed to date. In addition to generating this new category of optical emissions, the completed HAARP array has caused the discovery of many other new and as yet unexplained heating effects. Since the array has been complete only since 2007, a large data set of optical effects at this high-power level does not exist. However, in the 2 week span of the October 2008 campaign, there were several clear nights of airglow observations, and the fine structure reported in this paper was only generated on the night of 28 October.

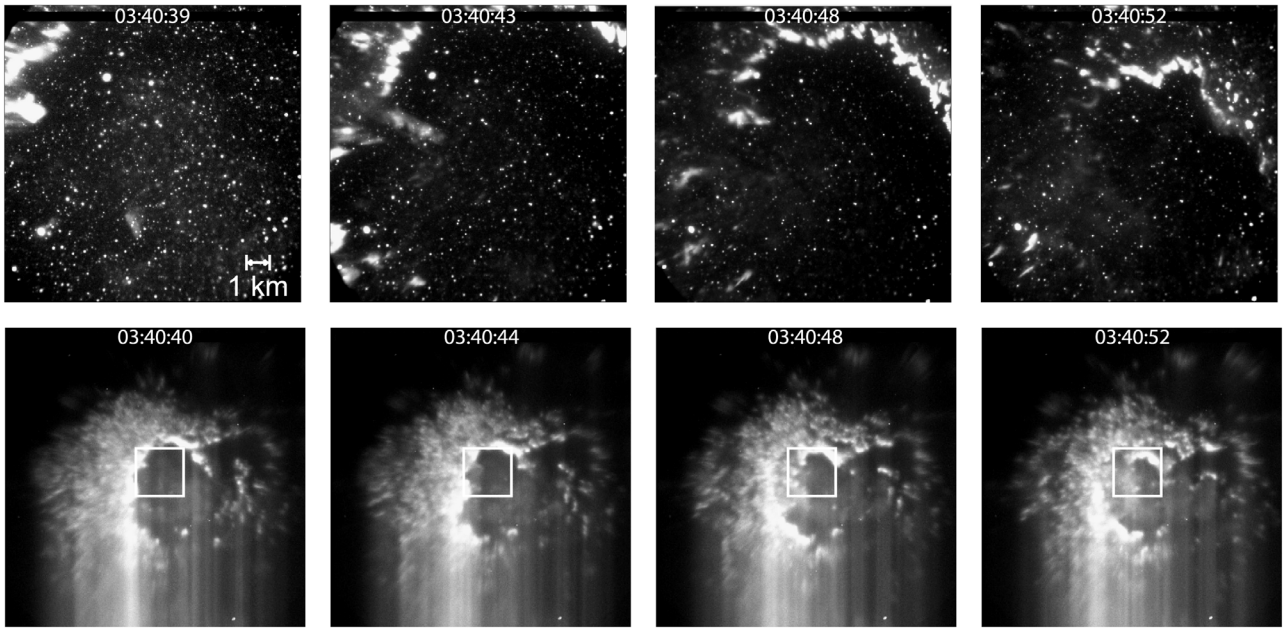

Figure 5. Clumps of rays were observed to move in arcs across the images. The top row shows the images from the telescope (~3°), and the bottom row shows images from the wide field of view camera (~19°). The telescope's view within the wide field of view is estimated by the white boxes. The vertical streaks seen in the wide field of view images are a camera artifact because of lack of shuttering and are not related to the airglow.

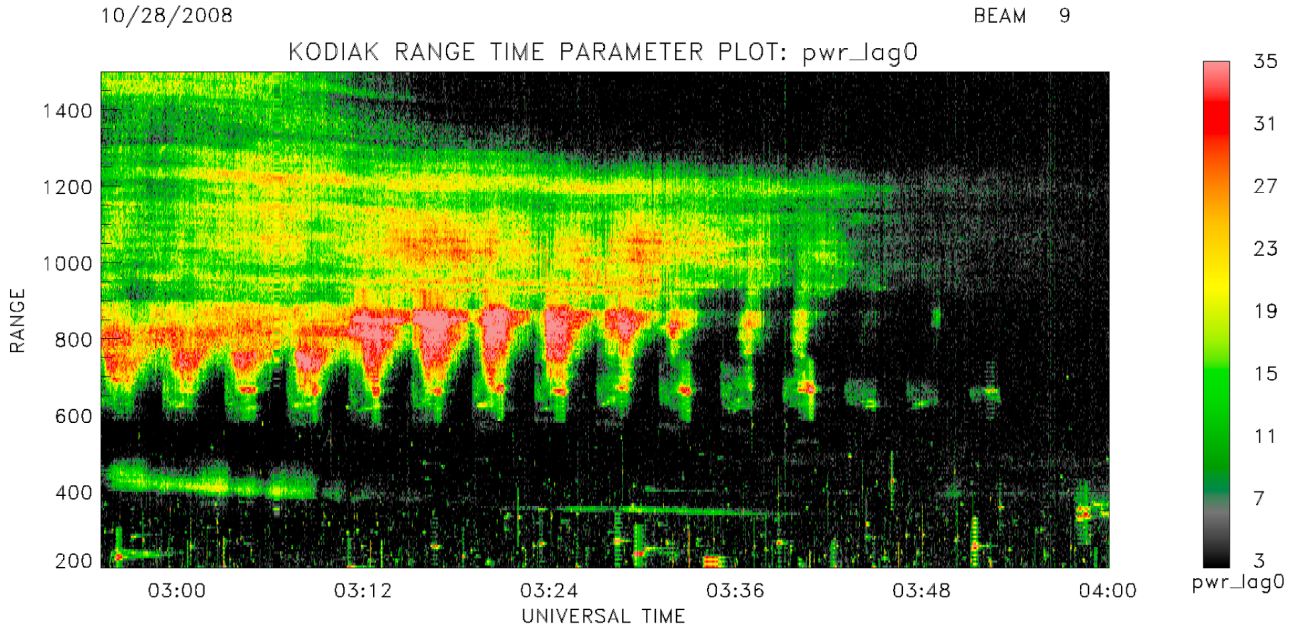

Figure 6. Range-time-intensity plot of beam 9 from the Kodiak SuperDARN radar data on 28 October. The radar switched between 10.6 and 13.6 MHz with beam widths of ~4.3° and ~3.4°, respectively. The backscatter at long ranges is due to natural irregularities. The scatter from ~600 to 900 km range intersects the HAARP beam and clearly shows the heating pulse pattern. Unlike the typical subsecond turn-on times, this scatter takes up to a minute to reach maximum intensity at some ranges.

[17] High-latitude heating experiments do not occur under controlled steady state conditions but rather in a turbulent dynamic environment. The 28 October was preceded by 10 days of quiet geomagnetic conditions with a *Kp* index of less than 2. Disturbance Storm Time index did not fall below −20 nT for this entire period. On 29 October, there was a small disturbance that lasted until 1 November, with *Kp* reaching 4.3. On the Gakona magnetometer (operated by the Geophysical Institute, University of Alaska), the quiet period was characterized by oscillations less than 50 nT and during the small disturbance, up to ~300 nT. Similarly, the HAARP riometer recorded ionospheric absorption less than 0.4 dB during the quiet interval and up to 2 dB during the disturbed period.

[18] On the night of 28 October, the HAARP ionosonde showed spread *F* occurring at dusk, indicating the presence of irregularities in the area. There was a double-hop echo at twice the virtual range because of the very low ionospheric absorption, verified by the HAARP 30 MHz riometer. The spread *F* persisted during the period of the experiment (0255–0400 UT) as f_oF_2 dropped from ~3 to ~2.4 MHz, well below HAARP's minimum operating frequency. An *E* layer was present, with a critical frequency up to ~2.3 MHz at 100 km virtual range. While the HAARP Modular UHF Ionospheric Radar (MUIR) incoherent scatter radar (ISR) was not operated in a useful mode for this particular experiment, the previous experiment at 0241 UT indicated an *F* region interaction altitude of ~204 km with a heating frequency of 2.85 MHz [C. Fallen, personal communication].

[19] Other instruments also recorded unusual effects during the 0255–0400 UT 28 October 2009 heating experiment. The Kodiak SuperDARN radar [*Greenwald et al.*, 1985; *Greenwald et al.*, 1995; *Hughes et al.*, 2003] observed coherent backscatter on its beam 9 which overlooks the HAARP array. During this experiment, the Kodiak radar had a range resolution of 6 km (13 bit Barker code) and 1 s integration. The radar switched between 10.6 and 13.6 MHz with beam widths of ~4.3° and ~3.4°, respectively. At 650 km range, the approximate distance between the radar and HAARP, the beam width is ~50 km at 10.6 MHz and ~40 km at 13.6 MHz. Figure 6 shows a plot of the backscattered power versus range and time for 0255–0400 UT. The HAARP backscatter is observed between ~600 and 900 km in range on this plot as determined by the correlation with HAARP's on and off transmission cycle. The ~300 km of range is much larger than that of the HAARP beam itself and could be due to the multiple altitudes of heater interaction (as evidenced in the ionosonde data) or possibly a result of HAARP's sidelobes. *Pedersen et al.* [2009] demonstrated that the HAARP beam could be refracted by increased levels of electron density in the center of the beam because of ionization from the heater. This refraction would cause HAARP to interact with a region larger than its beam width and could explain the large backscattering region apparent in the SuperDARN data. The backscatter at larger ranges is from naturally occurring irregularities. Since this experiment occurred at twilight, the ionosphere was quickly decaying and f_oF_2 dropped rapidly. At around 0348 UT, the radar signal faded away. The Kodiak SuperDARN operator switched to a different frequency to see if propagation effects were the cause of the signal loss, but the backscatter did not increase. This implies that the signal loss was due to the irregularities (either natural or heater-induced) fading away.

[20] While there is an obvious HAARP signature of 2 min on/off in the SuperDARN data, the pattern is unlike that typically observed during heating experiments. An example

of previously observed HAARP-induced backscatter during artificial optical emission can be seen in the study of *Kosch et al.* [2005]. The first unusual feature is the relatively gradual rise time of the backscatter pulses. Figure 7 shows slices in range across the range-time-intensity plot of Figure 6. Although this is a rough proxy indicator of the time it took irregularities to form, it is evident that some features are developing on the order of tens of seconds and up to a minute not the subsecond rise time that is expected [*Wright et al.*, 2006; *Hughes et al.*, 2003]. This slow development is in line with the time scale for the production of "artificial ionospheric layers" as detailed by *Pedersen et al.* [2010].

[21] Another atypical feature observed in the SuperDARN data is the presence of a small region of backscatter at ~650 km range lasting for a minute or less. Backscatter at this short range continues to be produced after the backscatter at larger ranges has faded away and roughly lines up with the appearance of the rays in the airglow data.

[22] GPS satellite data also captured HAARP heating effects during this experiment. Figure 8 shows data from satellite 21 collected by the GNAA receiver in Glennallen, Ak (62°N, 214°E) operated by NOAA. When the satellite was over the HAARP-heated region, peaks in the vertical TEC data occurred from ~0300 to 0325 UT correlated with the heater on/off cycle. While these peaks were only on the order of tenths of a TEC unit, they are clearly visible in the data. The bottom plot in Figure 8 shows the detrended data with the approximate background level subtracted. While there are only 7–9 samples per heating cycle, it is still evident that the TEC level takes a minute or longer to rise to its maximum value. This differs from the subsecond time scales previously observed in heater-related TEC fluctuations [*Milikh et al.*, 2008] and is more in line with the time scales of "artificial ionospheric layer" formation [*Pedersen et al.*, 2010].

[23] A direct-sampling receiver for recording stimulated electromagnetic emissions (SEEs) was operated in Gakona (~20 km from the HAARP site) by the Naval Research Laboratory. These receiver data were processed over a range of frequency resolutions making spectral measurements of emissions from kHz down to only a few Hz away from the transmitted heating frequency. As the evening progressed on 28 October, the SEE spectra changed with the changing ionospheric conditions. A one-to-one relationship between the spectra and the airglow features observed is not readily produced; however, some bulk properties can be related. This is a rich data set that will be investigated under a different study. At 0243 UT, the SEE spectra showed strong lines shifted ~120–360 Hz down from the main transmitter signal, and these lines have been interpreted as the ion-Bernstein mode. These lines were not observed prior to HAARP power upgrade to completion but are now a regular feature in the SEE spectra at HAARP when the transmitter is tuned to the second harmonic of the electron cyclotron frequency near the reflection altitude. The lines lasted until ~0341 UT which is when the airglow and the SuperDARN backscatter began to fade. A downshifted maximum (DM) was also present at 0243 UT but was gone by 0339 UT. The DM shifted from 7.7 to 6.0 kHz below the main transmitter line during this period. The DM is associated with irregularities and commonly observed during spread *F* conditions [*Leyser*, 2001]. From ~0243–0341 UT, an upshifted ledge was observed extending to 10 Hz above the transmitter signal. This maximum value of this peak slowly increased from −60 to −48 dB until the 0339–0340 UT pulse when it grew from −80 to −35 dB and was stronger than the transmitter signal. This peak is thought to be the result of the oscillating two-stream instability [*Dysthe et al.*, 1983]. Finally at ~0355 UT, when the airglow has completely faded away, a peak is observed at −31 Hz that builds with time to nearly the strength of the transmitter pulse. This peak is attributed to ion-acoustic wave from stimulated Brillouin scatter (SBS) [*Bernhardt et al.*, 2009; *Norin et al.*, 2009] and is particularly strong. SBS is thought to occur when the *O*-mode electromagnetic wave decays into an ion-acoustic wave and a scattered electromagnetic wave and may happen when the HF slightly exceeds the local plasma frequency if the HF power is large [*Bernhardt et al.*, 2009], an interpretation in agreement with the rest of this particular data set.

4. Discussion

[24] The 100 m scale artificial airglow observed on 28 October 2008 is thus far a unique observation and the smallest-scale size heater-induced airglow reported to date. Unique observations are not entirely unexpected for several reasons. Historically, airglow observations have been made by medium to all-sky field of view cameras, while the HAARP telescope field of view is only 3° wide and thus able to capture fine structure which may go undetected on other systems. The HAARP facility was only completed in 2007, and few optical campaigns have been run at full power, opening the door to a whole host of discoveries. On top of these limiting factors, during any particular campaign, the odds of generating useful airglow are restricted by the need for clear dark skies, little moonlight, low ionospheric absorption, f_oF_2 above the lowest transmitting frequency, and relatively quiet geomagnetic conditions, although there have been exceptions to this rule of thumb [*Pedersen and Gerken*, 2005].

[25] The cause of this unprecedented observation is as yet unknown. One possible explanation is tied to the location of the plasmapause footprint with respect to HAARP during the experiment. *Greenwald et al.* [2006] observed decameter-scale irregularities in SuperDARN data from Wallops Island, Va, and after investigation concluded that they were due to the thermal gradient instability (TGI). TGI takes place where there are opposing temperature and density gradients and is predicted to occur in the ionospheric footprint of the plasmapause region, on the equatorward ionospheric trough boundary. In the study of Greenwald et al., this conjecture was backed by Millstone Hill ISR data; however, that capability is not present at the HAARP facility. The features displayed in the study of Greenwald et al. are remarkably similar to those observed in the 28 October Kodiak natural backscatter at ranges beyond HAARP (Figure 6), and decameter features were also observed in the airglow data (e.g., Figure 3). Since the geomagnetic conditions were very quiet before the 28 October observations, the HAARP geomagnetic field line would likely cross the equatorial plane around 5 R_E. At 0300 UT, HAARP is located at 16.5 magnetic local time. Under these conditions and at this time, it is probable

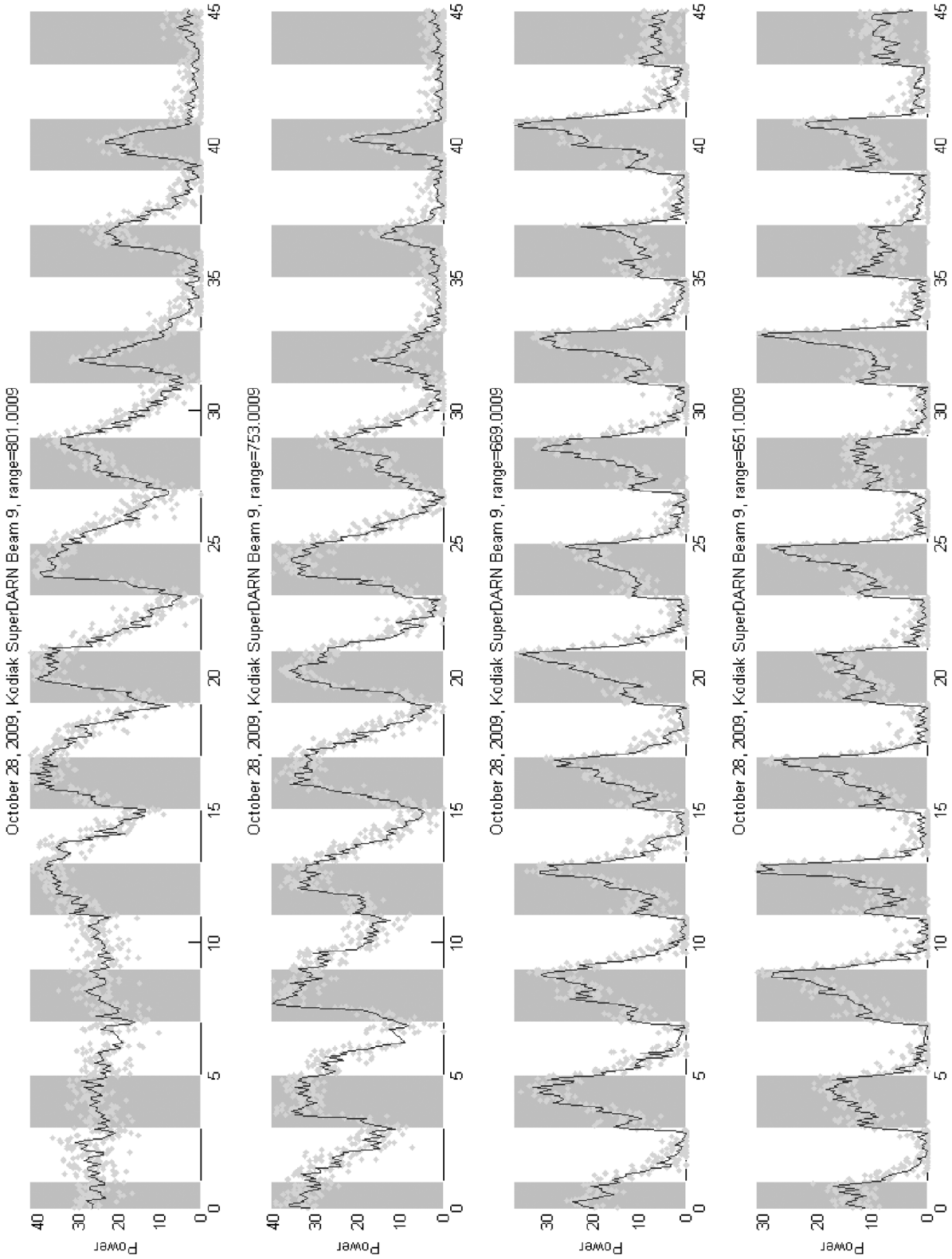

Figure 7. Kodiak SuperDARN beam 9 data from individual range gates. The gray bars indicate heater-on times. The light gray dots are the raw SuperDARN data, and the dark gray line is an averaged version of the data. All the ranges show some onset delay; however, the closest ranges show the longest delays.

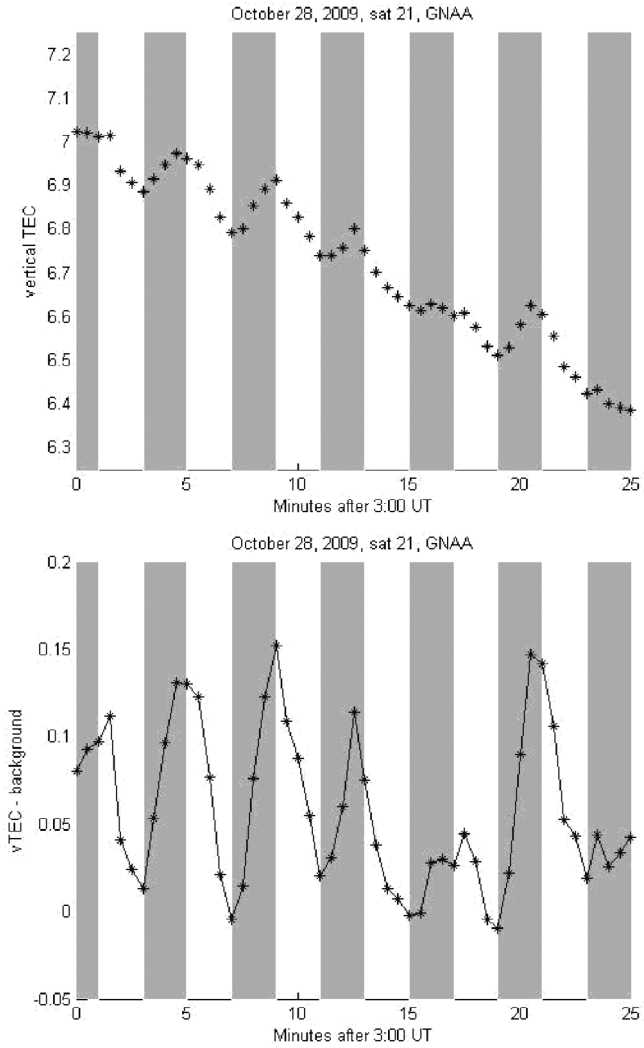

Figure 8. GPS satellite 21 vertical TEC data from the GNAA receiver. The light gray bars show the heater-on periods. (top) Vertical TEC data. (bottom) Data are detrended with the background TEC subtracted. The vertical TEC fluctuates with the heater pulse, rising during the entire pulse interval rather than rising quickly as previously observed in heater-related TEC fluctuations.

that HAARP was within the plasmapause, so the TGI could be a factor in the generation of the decameter features observed in the HAARP airglow. GPS TEC data affirm this conjecture and show that HAARP is located very close to the ionospheric footprint of the plasmapause. Figure 9 shows the global zenith TEC in bins of 2° latitude and 2° longitude calculated from the worldwide network of GPS receivers using the method described in the study of *Rideout and Coster* [2006]. A white dot demarks the location of the HAARP facility. The location of HAARP is clearly shown to sit on a rather sharp boundary in the TEC values, from 7 to 8 TEC units indicated by red to 1 to 2 TEC units indicated by blue. This drop in TEC corresponds to the location of the plasmaspheric boundary layer. The likely presence of the plasmapause footprint in the HAARP vicinity is further supported by the empirical model published by *Carpenter and Anderson* [1992].

[26] Both the presence of the 427.8 nm emission and the change in TEC as observed by GPS indicate that ionization may be occurring during this experiment. Enhancements at 427.8 nm imply the presence of ionization and were first observed at EISCAT by *Holma et al.* [2006] and later by *Gustavsson et al.* [2006]. *Holma et al.* [2006] demonstrated that wideband photometer measurements of 427.8 nm detect not only N_2^+(1 NG) emissions but also a significant contribution from N_2(2 P) and a slight amount of N_2(Vegard-Kaplan). The N_2^+ (1 NG) emission has an excitation threshold of 18.6 eV and the N_2(2 P) has a threshold of 11.2 eV. The O_2 ionization threshold is 12.8 eV and the N_2 ionization threshold is 15.6 eV, which means that an observation of N_2^+(1 NG) implies ionization. As previously described, in the 28 October telescope images, initial diffuse airglow appears within seconds of heater turn-on and then after tens of seconds, the brighter rays develop. It appears that these two processes may be decoupled in the spectral features captured by the Stanford/HAARP photometer. Unlike the 630.0, 557.7, 777.4, and 844.6 nm emissions, prior to 0335 UT, the 427.8 nm line peaks within a second of the heater turning on and then begins to decay (Figure 4). On the 0335 and 0340 UT pulses, the 427.8 nm pulse increases more similarly to the other lines. This indicates that while the diffuse initial airglow contained 427.8 nm emissions, the rays did not, or at least not at the same intensity. *Gustavsson et al.* [2006] also noted a difference between the 630 and 427.8 nm airglow emissions and conjectured that different processes were involved. The GPS data do not exhibit the same temporal variation as the 427.8 nm photometer data but rather are more similar to

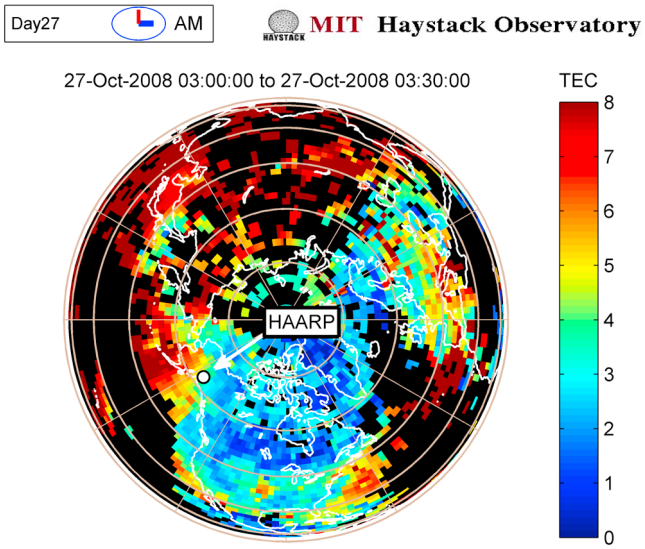

Figure 9. The global zenith total electron content (TEC) in bins of 2° latitude and 2° longitude calculated from the worldwide network of GPS receivers using the method described in the study of *Rideout and Coster* [2006]. A white dot demarks the location of the HAARP facility. The location of HAARP is clearly shown to sit on a rather sharp boundary in the TEC values, from 7 to 8 TEC units indicated by red to 1 to 2 TEC units indicated by blue. This drop in TEC corresponds to the location of the plasmaspheric boundary layer.

the 557.7 nm data and peak at the end of each heater-on pulse. This discrepancy is not unexpected since the GPS data are directly measuring ionization effects, while the photometer is measuring the 427.8 nm emission that is due to a higher energy process. It may be that the heating initially spikes to maximum electron energies above the 427.8 emission threshold (18.6 eV) and then decreases as the pulse continues or perhaps that the electron flux above the threshold is varying. Thus, while ionization would occur during the entire pulse, as evidenced by the TEC data, the heating would only be high enough to cause the 427.8 nm emission at the beginning of the pulse.

[27] Turbulence “”because of a variety of heater-induced plasma instabilities is predicted to form field-aligned irregularities on a number of spatial and temporal scales. Thermal resonant instability is expected to generate upper hybrid plasma turbulence, which produces irregularities with scale sizes on the order of 30–50 m within the first second of heating [*Milikh et al.*, 2008]. In the next 10–30 s, 0.1–1 km scale irregularities should form because of a self-focusing instability [*Gurevich et al.*, 1996]. Eventually, these irregularities are predicted to become larger than 1–2 km “”because of magnification of natural irregularities [*Milikh et al.*, 2008]. In contrast to these predictions, however, the airglow presented in this paper started out large scale and became more structured about a minute into the pulse. In fact, the structure may have developed even more if the pulses had been lengthened. One aspect that does match current theory, however, is that when features such as arcs were observed (Figure 5), the arcs were semicircular, and they are composed of small-scale irregularities. *Istomin and Leyser* [2003] predict cylindrical structuring of irregularities with the cylinders composed of smaller-scale irregularities. This was also observed on another night during the campaign (not presented here). This effect is predicted to occur at pump frequencies slightly above an electron gyroharmonic frequency. The ionosonde data in Figure 2 show this was true in the *F* region at 0340 UT, the time of the arcs in the Figure 5.

[28] Although the observations presented are informative in and of themselves, several improvements can be made for future experiments. The most glaring gap in the data set is a lack of any side-viewing imagery, which can show the vertical structure of these features. It is possible that the diffuse regions and bright rays could in fact be generated in two different regions of the ionosphere and be due to two separate mechanisms. The HAARP Optical Observing Network [*Pedersen et al.*, 2008] provides such data for HAARP observations; however, on this particular night, it was not in operation. If the MUIR radar at HAARP were operated in a long coded pulse mode, it should be able to capture height-resolved backscatter for the *F* region if the signal were particularly strong, but on this particular night, the radar was run only in an uncoded long pulse mode [B. Watkins, personal communication, 2009]. Another improvement that could be made to this experiment would be to lengthen the transmission pulse. As seen clearly in the photometer data (Figure 4), the airglow signal was still rising when the transmitter was turned off after 2 min. It is possible that with a longer pulse sequence, the rayed features would further develop and more information could be gleaned from the results.

[29] **Acknowledgments.** Data for the basis of this paper were acquired through support from the High frequency Active Auroral Research Program (HAARP), jointly managed by the United States Air Force and Navy. E. Kendall’s efforts were supported through funding by the Office of Naval Research grant N00014-05-C-0369. The HAARP research at the Naval Research Laboratory was funded by the Office of Naval Research.

[30] Robert Lysak thanks John Hughes and Mike Kosch for their assistance in evaluating this paper.

References

Adeishvili, T. G., A. V. Gurevich, S. B. Lyakhov, G. G. Managadze, G. M. Milikh, and I. S. Shlyuger (1979), Ionospheric emission caused by an intense radio wave, *Sov. J. Plasma Phys.*, *4*, 721.

Ashrafi, M., M. J. Kosch, and F. Honary (2006), Heater-induced altitude descent of the EISCAT UHF ion line enhancements: observation and modelling, *Adv. Space Res.*, *38*, 2645.

Ashrafi, M., M. J. Kosch, K. Kaila, and B. Isham (2007), Spatiotemporal evolution of radio wave pump-induced ionospheric phenomena near the fourth electron gyroharmonic, *J. Geophys. Res.*, *112*, A05314, doi:10.1029/2006JA011938.

Bernhardt, P. A., L. M. Duncan, and C. A. Tepley (1989), Heater-induced cavities as optical tracers of plasma drifts, *J. Geophys. Res.*, *94*(A6), 7003–7010, doi:10.1029/JA094iA06p07003.

Bernhardt, P. A., W. A. Scales, S. M. Grach, A. N. Keroshtin, D. S. Kotik, and S. V. Polyakov (1991), Excitation of artificial airglow by high-power radio waves from the “SURA” ionospheric heating facility, *Geophys. Res. Lett.*, *18*, 1477.

Bernhardt, P. A., M. Wong, J. D. Huba, B. G. Fejer, L. S. Wagner, J. A. Goldstein, C. A. Selcher, V. L. Frolov, and E. N. Sergeev (2000), Optical remote sensing of the thermosphere with HF pumped artificial airglow, *J. Geophys. Res.*, *105*(A5), 10,657–10,671, doi:10.1029/1999JA000366.

Bernhardt, P. A., C. A. Selcher, R. H. Lehmberg, S. Rodriguez, J. Thomason, and M. McCarrick (2009), Gordon Frazer determination of the electron temperature in the modified ionosphere over HAARP using the HF pumped stimulated Brillouin scatter (SBS) emission lines, *Ann. Geophys.*, (in press).

Biondi, M. A., D. P. Sipler, and R. D. Hake Jr. (1970), Optical (λ6300) detection of radio frequency heating of electrons in the *F* region, *J. Geophys. Res.*, *75*, 6421.

Brändström, B. U. E., T. B. Leyser, Å. Steen, M. T. Rietveld, B. Gustavsson, T. Aso, and M. Ejiri (1999), Unambiguous evidence of HF pump-enhanced airglow at auroral latitudes, *Geophys. Res. Lett.*, *26*, 3561.

Carpenter, D. L., and R. R. Anderson (1992), An ISEE/Whistler model of equatorial electron density in the magnetosphere, *J. Geophys. Res.*, *97*, 1097.

Djuth, F. T., et al. (1999), Large airglow enhancement produced via wave-plasma interactions in sporadic E, *Geophys. Res. Lett.*, *26*, 1557.

Djuth, F. T., T. R. Pedersen, E. A. Gerken, P. A. Bernhardt, C. A. Selcher, W. A. Bristow, and M. J. Kosch (2005), Ionospheric modification at twice the electron cyclotron frequency, *Phys. Rev. Lett.*, *94*, 125001.

Dysthe, K. B., E. Mjolhus, K. Rypdal, and H. L. Pecseli (1983), A thermal oscillating two-stream instability, *Phys. Fluids*, *26*, 146.

Greenwald, R. A., K. B. Baker, R. A. Hutchins, and C. Hanuise (1985), An HF phased-array radar for studying small-scale structure in the high-latitude ionosphere, *Rad. Sci.*, *20*, 63.

Greenwald, R. A., K. B. Baker, J. R. Dudeney, and M. Pinnock (1995), DARN/SuperDARN: A global view of the dynamics of high-latitude convection, *Space Sci. Rev.*, *71*, 761.

Greenwald, R. A., K. Oksavik, P. J. Erickson, F. D. Lind, J. M. Ruohoniemi, J. B. H. Baker, and J. W. Gjerloev (2006), Identification of the temperature gradient instability as the source of decameter-scale ionospheric irregularities on plasmapause field lines, *Geophys. Res. Lett.*, *33*, L18105, doi:10.1029/2006GL026581.

Gurevich, A. V., A. V. Lukyanov, and K. P. Zybin (1996), Anomalous absorption of powerful radio waves on the striations developed during ionospheric modification, *Phys. Lett. A*, *211*, 363.

Gustavsson, B., et al. (2001), First tomographic estimate of volume distribution of HF-pumped enhanced airglow emission, *J. Geophys. Res.*, *106*, 29,105–29,123, doi:10.1029/2000JA900167.

Gustavsson, B., T. B. Leyser, M. Kosch, M. T. Rietveld, Å. Steen, B. U. E. Brändström, and T. Aso (2006), Electron gyroharmonic effects in ionization and electron acceleration during high-frequency pumping in the ionosphere, *Phys. Rev. Lett.*, *97*, 195002.

Holma, H., K. U. Kaila, M. J. Kosch, and M. T. Rietveld (2006), Recognizing the blue emission in artificial airglow, *Adv. Space Res.*, *38*, 2653.

Hughes, J. M., W. A. Bristow, and R. T. Parris (2003), SuperDARN observations of ionospheric heater-induced upper hybrid waves, *Geophys. Res. Lett.*, *30*(24), 2276, doi:10.1029/2003GL018772.

Istomin, Y. N., and T. B. Leyser (2003), Electron acceleration by cylindrical upper hybrid oscillations trapped in density irregularities in the ionosphere, *Phys. Plasmas*, *10*, 2962.

Kagan, L. M., M. C. Kelley, F. Garcia, P. A. Bernhardt, F. T. Djuth, M. P. Sulzer, and C. A. Tepley (2000), The structure of electromagnetic wave-induced 557.7-nm emissions associated with a sporadic-E event over Arecibo, *Phys. Rev. Lett.*, *85*, 218.

Kelley, M. C. (1989), *The Earth's Ionosphere*, Academic, San Diego, Calif.

Kelley, M. C., T. L. Arce, J. Salowey, M. Sulzer, W. T. Armstrong, M. Carter, and L. Duncan (1995), Density depletions at the 10 m scale induced by the Arecibo heater, *J. Geophys. Res.*, *100*(A9), 17,367–17,376, doi:10.1029/95JA00063.

Kosch, M. J., M. T. Rietveld, T. Hagfors, and T. B. Leyser (2000), High-latitude HF-induced airglow displaced equatorwards of the pump beam, *Geophys. Res. Lett.*, *27*(17), 2817–2820, doi:10.1029/2000GL003754.

Kosch, M. J., M. T. Rietveld, A. Senior, I. W. McCrea, A. J. Kavanaugh, B. Isham, and F. Honary (2004), Novel artificial optical annular structures in the high latitude ionosphere over EISCAT, *Geophys. Res. Lett.*, *31*, L12805, doi:10.1029/2004GL019713.

Kosch, M. J., T. Pedersen, J. Hughes, R. Marshall, E. Gerken, A. Senior, D. Sentman, M. McCarrick, and F. T. Djuth (2005), Artificial optical emissions at HAARP for pump frequencies near the third and second electron gyroharmonic, *Ann. Geophys.*, *23*, 1585.

Leyser, T. B. (2001), Stimulated electromagnetic emissions by high-frequency electromagnetic pumping of the ionospheric plasma, *Space Sci. Rev.*, *98*, 223.

Milikh, G., A. Gurevich, K. Zybin, and J. Secan (2008), Perturbations of GPE signals by the ionospheric irregularities generated due to HF-heating at triple of electron gyrofrequency, *Geophys. Res. Lett.*, *35*, L22102, doi:10.1029/2008GL035527.

Norin, L., T. B. Leyser, E. Nordblad, B. Thidé, and M. McCarrick (2009), Unprecedentedly strong and narrow electromagnetic emissions stimulated by high-frequency radio waves in the ionosphere, *Phys. Rev. Lett.*, *102*, doi:10.1103/PhysRevLett.102.065003.

Pedersen, T. R., and H. C. Carlson (2001), First observations of HF heater-produced airglow at the High Frequency Active Auroral Research Program Facility: thermal excitation and spatial structuring, *Radio Sci.*, *36*, 1013–1026, doi:10.1029/2000RS002399.

Pedersen, T., M. McCarrick, E. Gerken, D. Sentman, A. Gurevich, and H. C. Carlson (2003), Magnetic zenith enhancement of artificial airglow production at HAARP, *Geophys. Res. Lett.*, *30*(4), 1169, doi:10.1029/2002GL016096.

Pedersen, T., and E. Gerken (2005), Naked eye visible artificial optical emissions created in the aurora by high-power radio waves, *Nature*, *433*, 498.

Pedersen, T., R. Esposito, E. Kendall, D. Sentman, M. Kosch, E. Mishin, and R. Marshall (2008), Observations of artificial and natural optical emissions at the HAARP facility, *Ann. Geophys.*, *26*, 1089.

Pedersen, T., B. Gustavsson, E. Mishin, E. MacKenzie, H. C. Carlson, M. Starks, and T. Mills (2009), Optical ring formation and ionization production in high-power HF heating experiments at HAARP, *Geophys. Res. Lett.*, *36*, L18107, doi:10.1029/2009GL040047.

Pedersen, T., B. Gustavsson, E. Mishin, E. Kendall, T. Mills, H. C. Carlson, and A. L. Snyder (2010), Creation of artificial ionospheric layers using high-power HF waves, *Geophys. Res. Lett.*, *37*, L02106, doi:10.1029/2009GL041895.

Rideout, W., and A. Coster (2006), Automated GPS processing for global total electron content data, *GPS Solut.*, doi:10.1007/s10291-006-0029-5.

Rodriguez, P., C. L. Siefring, D. G. Haas, P. A. Bernhardt, and M. M. Baumback (1995), Evidence of HF-driven wave interactions in the ionospherics focused heating experiment, *Geophys. Res. Lett.*, *22*(23), 3251–3254, doi:10.1029/95GL02778.

Sentman, D., R. Wuerker, M. McCarrick, T. Pedersen, E. Wescott, H. Stenbaek-Nielsen, A. Wong, M. Kubota, F. Sao Sabbas, and D. Lummerzheim (2002), Imaging and spectrographic observations of artificial airglow excited by HAARP and HIPAS, 34th COSPAR Scientific Assembly, The Second World Space Congress, held 10–19 October, 2002, in Houston TX, USA, meeting abstract.

Sipler, D. P., and M.A. Biondi (1972), Measurements of O(^1D) quenching rates in the F region, *J. Geophys. Res.*, *77*, 6202.

Sipler, D. P., E. Enemark, and M. A. Biondi (1974), 6300-intensity variations produced by the Arecibo ionospheric modification experiment, *J. Geophys. Res.*, *79*, 4276.

Stubbe, P., et al. (1982), Ionospheric modification experiments in northern Scandinavia, *J. Atmos. Terr. Phys.*, *44*, 1025.

Wright, D. M., J. A. Davies, T. K. Yeoman, T. R. Robinson, and H. Shergill (2006), Saturation and hysteresis effects in the ionospheric modification experiments observed by the CUTLASS and EISCAT radars, *Ann. Geophys.*, *24*, 543.

P. Bernhardt and C. Selcher, Plasma Physics Division, Naval Research Laboratory, Code 6754, 4555 Overlook Avenue, SW Washington, DC 20375-0001, USA.

A. Bhatt and A. Coster, Haystack Observatory, Massachusetts Institute of Technology, Route 40, Westford, MA 01886-1299, USA.

E. Kendall, SRI International, 333 Ravenswood Avenue, Menlo Park, CA 94025-3493, USA. (elizabeth.kendall@sri.com)

R. Marshall, Stanford University, 350 Serra Mall, Stanford, CA 94305-9515, USA.

R. T. Parris, University of Alaska, 903 Koyukuk Drive, 713A, Fairbanks, AL 99775, USA.

T. Pedersen, Air Force Research Laboratory, 29 Randolph Road, Hanscom AFB, MA 01731-2002, USA.